Adsorption of pyridine from aqueous solutions by polymeric adsorbents MN 200 and MN 500. Part 2: Kinetics and diffusion analysis

Qingyu Zhu, Geoff D. Moggridge*, Carmine D'Agostino*

***Corresponding authors:**

Dr Carmine D'Agostino

Address: Department of Chemical Engineering and Biotechnology, University of Cambridge, Pembroke Street, Cambridge, CB2 3RA, UK

Email: cd419@cam.ac.uk

Telephone: +44 (0)1223 761628

Fax: +44 (0)1223 334796

Dr Geoff Moggridge

Address: Department of Chemical Engineering and Biotechnology, University of Cambridge, Pembroke Street, Cambridge, CB2 3RA, UK

Email: gdm14@cam.ac.uk

Telephone: +44 (0)1223 334763

Fax: +44 (0)1223 334796

Abstract

The adsorption kinetics of pyridine adsorption on Macronet adsorbents MN 200 and MN 500 from aqueous solution was investigated at various initial pyridine concentrations and temperatures. The Weber-Morris plots revealed the influence of both external film diffusion and intraparticle diffusion resistances. The two linear regions in Weber-Morris plots were attributed to macropore and micropore diffusion, which was associated to the bimodal pore size distribution of the adsorbents. New insights into the diffusion mechanisms were highlighted, with the proposed internal film diffusion resistance dominating into the macropore region, whereas homogeneous particle diffusion resistance describes diffusion in the micropore region. The importance of pore and surface diffusion in the micropores was noted in contributing to the observed diffusion kinetics. The pore diffusion coefficient was estimated from PFG (pulsedfield gradient) parameter and molecular diffusion coefficient of pyridine in bulk liquid. A greater contribution of the surface to the overall diffusion kinetics was found for MN 500 as inferred from a proposed calculation method, which agrees with its better adsorption performance. The overall findings highlight the effect of pore structure onto the diffusion mechanisms inside the pores and help to gain a better understanding into the adsorption kinetics of these Macronet adsorbents, which are promising materials for the removal of N-heterocyclic compounds from waste water.

Key words: Pyridine adsorption, Macronet adsorbents, adsorption kinetics, intraparticle diffusion, pore and surface diffusions

1. Introduction

Pyridine is a parent of a series of N-heterocyclic aromatic compounds that occur naturally in the environment and are also produced for the manufacturing of agricultural chemicals, dyestuffs and paints and other chemicals [1]. Pyridine compounds are hazardous in nature because of their toxic and carcinogenic potential and hazardous effects on environment and organisms even at low concentrations [2]. Because of their high water solubility, high volatility and long-time persistence in the environment, they are easily transported through the soil and water and are often detected in wastewater[3]. The removal of these compounds is of great importance to minimise damages to health and environment.

Adsorption of pyridine compounds from aqueous solutions is more frequently used compared to other processes such as biodegradation [4,5], pervaporation [6] and chemical oxidation [7,8]. Many studies have explored pyridine adsorption performance using porous materials including activated carbons [9–12], clayey till and zeolites [13,14], synthetic apatite [1], polymer resins [15,16], and metal organic frameworks [17,18].

Macronet materials present a hypercrosslinked polymeric structure providing controlled pore sizes and high surface areas [19]. These materials possess both macro- and micro-porosity at the same time, retained from their swollen-state in synthesis [20,21]. Macronet adsorbents MN 200 and MN 500 have recently been shown excellent performance for pyridine adsorption from aqueous solutions in batch experiments, where the enhanced adsorption rate and capacity were shown on MN 500, which can be attributed to the presence of sulfonic acid groups over the internal surface [22].

Adsorption kinetic is one basic requirement for optimal design of adsorption and separation processes. Adsorption of organic species on porous adsorbents in batch experiment can be described through a number of sequential processes acting in conjunction, including (a) the mass transport of adsorbate in bulk solution; (b) adsorbate diffusion through the liquid film towards the adsorbent particle (external film diffusion); (c) adsorbate diffusion within the adsorbent particle (intraparticle diffusion); and (d) van der Waals interaction (physisorption), or chemical reaction and other intermolecular interactions due to high

binding energies such as electrostatic and hydrogen bonding (chemisorption) within the adsorbent matrix. To understand the adsorption kinetics, an accurate rate expression is required for each mechanism in the process, which makes the overall kinetic model very difficult to evaluate. Typically, a proper agitation can reduce the resistance of adsorbate transport in solution and suppress the boundary layer around the adsorbent particles; hence, film diffusion on the external adsorbent surface will only affect the adsorption kinetics for a short initial period of time [19,23]. Chemical reaction or van der Waals interactions between the adsorbate and the adsorbent, in general, are not rate limiting unless chemical modifications prevalently occur during adsorption [24,25]. In most cases, intraparticle diffusion rate-controls the overall adsorption kinetics [24,26–29].

Many mathematical models have been developed for intraparticle diffusion of liquid adsorption on porous materials, attempting to understand adsorption kinetics in relation to the adsorbent pore structures and surface properties in terms of a constant diffusion coefficient assuming homogeneous pore property of the adsorbent [30–38]. Study of pore size heterogeneity revealed the variation of adsorbate diffusivity within the porous adsorbent [23,39,40]. These processes have been modelled as a fractal-like dependence of diffusion coefficient [34,41,42], or to involve correlated variables, by categorising the adsorption kinetics into macropore and micropore diffusional regions, respectively [32,39,43]. As a key element for assessing the adsorption performance, the importance of surface diffusion in contributing to the total adsorbent mass transfer in porous materials has been highlighted in many liquid-surface adsorption systems [44,45]. A number of models in determining surface diffusion coefficients are given in the literature, based on molecular hopping, hydrodynamic, Fick's, or combined theories [46], most of which showed joint contribution of pore and surface diffusions in the intraparticle diffusion processes [47–50].

In this work, diffusion mechanisms within the Macronet adsorbents will be thoroughly evaluated in order to elucidate the effect of adsorbent structural and surface properties on molecular motion within the pore space as well as adsorption performances, which complements the analysis of the Macronet adsorbents in the removal of pyridine from aqueous solutions in Part 1 [22]. For these adsorbents exhibiting bimodal

pore property in pore size, a new intraparticle diffusion mechanism will be proposed incorporating internal film diffusion in large pores and homogeneous particle diffusion for adsorbate motion in smaller pores. In addition, an equation for surface diffusion coefficient will be introduced based on the information of adsorption kinetics and pore geometry of adsorbents.

2. Materials and methods

The kinetic data for adsorption of pyridine on MN 200 and MN 500 are from the previously reported experimental results of batch reactor studies [22]. A weighed sample of adsorbent (63 mg) was poured into 50 mL pyridine aqueous solutions with an initial concentration of 150 mg/L and stirred at 600 rpm in a flask at controlled temperature. The adsorption kinetics was determined by analysing the remaining pyridine concentration in the reactor at certain time intervals at wavelength of ca 255 nm with a Shimazu 160A UV-vis spectrophotometer. The adsorption uptake over time, q (mg/L), is expressed as:

$$q = \frac{V(C_0 - C)}{m_s} \quad (1)$$

where C_0 and C are the initial and pyridine concentration and pyridine concentration at time t in solution (mg/L), V is the initial solution volume (L) and m_s is the adsorbent mass (g). The temperature and initial pyridine concentration dependence of pyridine uptake on the adsorbents were investigated by varying the temperature from 25-55 ^{0}C and initial pyridine concentration from 100-200 mg/L, respectively, with the other condition remaining constant. To have reliable results, the experiments were repeated for three times and the uncertainty was up to $\pm$10 %.

3. Results and discussion

3.1. Weber-Morris equation

Diffusion mechanisms of liquid-surface adsorption processes are typically characterised on the basis that one diffusion resistance is assumed to be predominant over other diffusion resistances. For the adsorption on synthetic polymers, the main diffusion resistance is likely to be film or intraparticle diffusion depending on the extend of polymer cross-linking [51]. To assess and differentiate the effect of film and intraparticle diffusion resistances on adsorption kinetics, the Weber-Morris equation, which was derived from Fick's law for adsorbent diffusing in spherical adsorbent particles at a short adsorption time, can be used to establish the relationship between the adsorbent uptake (q) and the square root of adsorption time ($t^{1/2}$) [52] as:

$$q = kt^{1/2} + I \tag{2}$$

The gradient (k) is defined as a diffusion rate parameter ($mgL^{-1}s^{-1/2}$). The value of the intercept (I), extrapolated from the initial linear portion of the plot back to the y-axis, is linked to the apparent thickness of the film boundary layer [53]. If an adsorption process is solely governed by intraparticle diffusion, the initial part of Weber-Morris plot is a straight line passing through the origin [54,55]. A negative value of the y-axis intercept in the equation indicates the effect of external film diffusion resistance [56]. A survey has shown positive intercepts for mostly organic compound adsorption on carbon materials [57], which can be attributed to a very fast initial adsorption uptake such that the initial data points cannot be immediately recorded in the experiments.

The Weber-Morris plots for pyridine uptake from aqueous solutions on MN 200 and MN 500 at various initial pyridine concentrations and temperatures are shown in Figures 1 and 2, respectively. In most cases, there is a time lag (hence a negative y-axis intercept) in the initial stage of the adsorption, which indicates that pyridine adsorption on both adsorbents experiences external film diffusion resistance. In addition, two different regimes for pyridine adsorption are observed, each of them showing linear behaviour, attributing to the intraparticle adsorption of pyridine into the adsorbent pores. This type of behaviour has been

frequently observed for adsorption of organic pollutants from water on various porous carbon materials [58–60] and functionalised hypercrosslinked polymers [61,62].

Macronet hypercrosslinked polymer adsorbents exhibit a bimodal pore size distribution with each maximum in the macroporous and microporous ranges [63]. This property can be reasonably associated to the two-component behaviour of PFG-NMR diffusion measurements of guest molecules in the adsorbents reported in Part 1 [22]. Since the gradient of the Weber-Morris plot carries information on kinetic properties, the observation of two linear diffusional regions can be plausibly ascribed to the bimodal pore size properties of the adsorbents. Therefore, it is plausible to assign the first linear region of the Weber-Morris plot to macropore diffusion, whereas the second accounts for micropore diffusion, each with a different gradient as a measure of diffusion rate constant (k).

The rate constants for macropore and micropore diffusion were determined by linear regression (using Equation 2) of the two regions, respectively, reported in Table 1. It is clearly shown that the diffusion rate constant (k) becomes significantly lower in the micropore region relative to the macropore region for both MN 200 and MN 500. A faster adsorption process of pyridine on MN 500 is noticed as the diffusion rate constants for pyridine adsorption on MN 500, especially in the macropore region, are larger relative to those on MN 200 at the same condition.

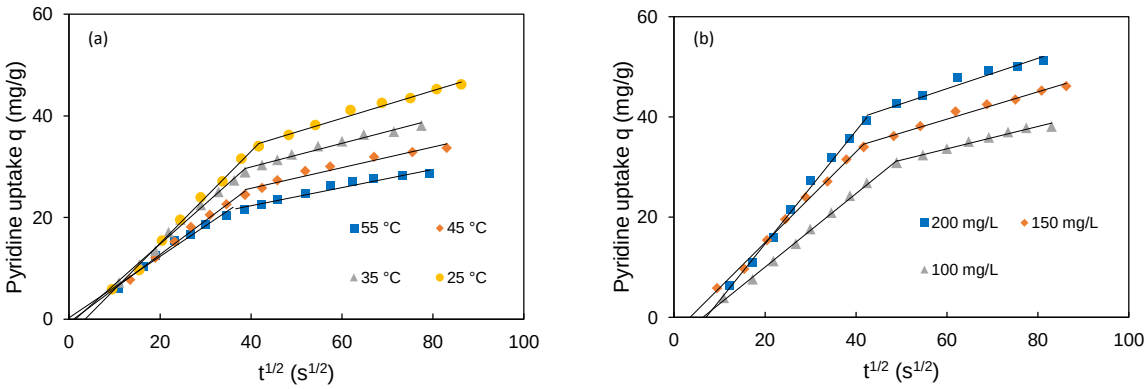

Figure 1. Weber-Morris plots on pyridine uptake on MN 200 by (a) varying temperature at initial pyridine concentration of 150 mg/L and by (b) varying the initial concentration at 25 ^{0}C. Uncertainty on the experimental data is up to $\pm$10%. The straight lines indicate linear regression of the two regions using Equation 2.

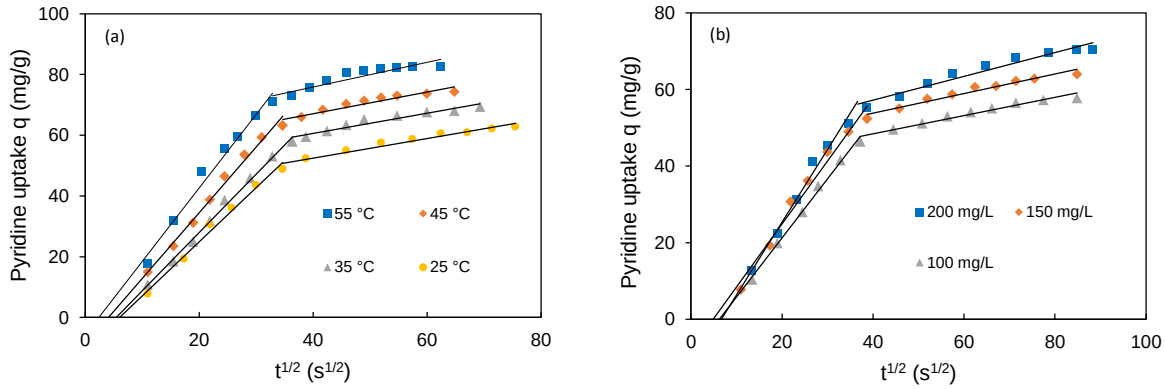

Figure 2. Weber-Morris plots on pyridine uptake on MN 500 by (a) varying temperature at initial pyridine concentration of 150 mg/L and by (b) varying the initial concentration at 25 ^{0}C. Uncertainty on the experimental data is up to $\pm$10%. The straight lines indicate linear regression of the two regions using Equation 2.

Table 1. Values of the diffusion rate parameter (k) for macropore and micropore regions and linear regression correlation coefficient (R^2) of the Weber-Morris plots for pyridine adsorption on MN 200 and MN 500 from aqueous solutions.

Adsorbent	T (^{0}C)	C_0 (mg /L)	macropore region		micropore region	
			k (mgL^{-1}s$^{-1/2}$)	R^2	k (mgL^{-1}s$^{-1/2}$)	R^2
MN 200	25	100	0.733$\pm$0.020	0.998	0.229$\pm$0.002	0.988
	25	150	0.905$\pm$0.035	0.996	0.272$\pm$0.006	0.985
	25	200	1.128$\pm$0.034	0.995	0.328$\pm$0.057	0.977
	35	150	0.812$\pm$0.029	0.991	0.239$\pm$0.004	0.970
	45	150	0.708$\pm$0.031	0.995	0.209$\pm$0.007	0.954
	55	150	0.665$\pm$0.055	0.982	0.243$\pm$0.005	0.985
MN 500	25	100	1.541$\pm$0.052	0.996	0.235$\pm$0.009	0.944
	25	150	1.645$\pm$0.226	0.978	0.240$\pm$0.020	0.966
	25	200	1.898$\pm$0.082	0.986	0.345$\pm$0.016	0.930
	35	150	1.922$\pm$0.047	0.995	0.290$\pm$0.009	0.943
	45	150	2.164$\pm$0.074	0.990	0.354$\pm$0.011	0.901
	55	150	2.420$\pm$0.179	0.983	0.393$\pm$0.227	0.861

T is temperature; C_0 denotes initial pyridine concentration in aqueous solutions.

Apart from the external film and intraparticle diffusion, the adsorbent-surface interaction (chemical or physical interaction) mechanism were examined in affecting the adsorption kinetics, though this is considered a fast process in most cases and negligible in limiting the adsorption of aromatic compounds onto hypercrosslinked polymeric adsorbents [58,61]. Because pyridine adsorption on MN 500 (functionalised with sulfonic acid groups) is shown to be an activated process, that is, the pyridine uptake increases with the increasing temperature [22], whether the surface-adsorbent interaction limits the adsorption process can be tested from the activation energy of diffusion, applying the Arrhenius equation with $ln(k)$ vs the reciprocal of temperature (T) as:

$$lnk = \frac{E_a}{RT} + lnA \tag{3}$$

where E_a is the activation energy of diffusion (kJ/mol), R is the gas constant and A is a pre-exponential factor. Plots of this equation were drawn for both the macropore and micropore regions shown in Figure 3. The activation energies of adsorption for the macropore and micropore regions, calculated from the gradients, are 10.4 and 12.6 kJ/mol respectively, both of which are in the range of 8-20 kJ/mol for diffusion controlled processes [53]. Therefore, it can be concluded that the adsorption-surface interaction is not rate-controlling in the adsorption process.

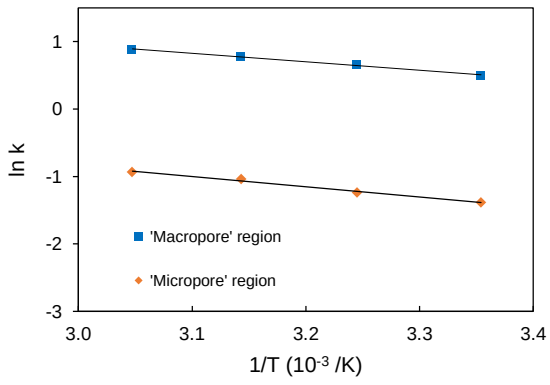

Figure 3. Arrhenius plots on the diffusion rate parameter k in the Weber-Morris equation for both macropore and micropore diffusion regions for pyridine adsorption on MN 500 from aqueous solutions.

3.2. Exploring intraparticle diffusion

Weber-Morris plots revealed negative intercepts for pyridine adsorption on MN 200 and MN 500 from aqueous solutions. This has often been encountered on the Macronet hypercrosslinked polymeric adsorbents, indicating film diffusion affected adsorption kinetics despite that the external film diffusion resistance was claimed to be removed or minimised by sufficient external agitation [58,64]. Because of the pore structure of the these adsorbents with the macropores being much larger relative to the size of the adsorbate molecules, the adsorbate is speculated to experience film diffusion resistance not only on the external adsorbent surface but also inside the large macropores*, i.e.,* a film exists between the bulk of the pore and the internal pore surface. Unlike external particle film diffusion, internal film in macropores cannot be sufficiently removed by external agitation. Application of film diffusion model (see Supporting Information) to the kinetics of pyridine adsorption on MN 200 and MN 500 shows that the internal film diffusion mechanism is able to describe the adsorption kinetics up to approximately 40 min for both MN 200 and MN 500, which is in line with the portion where the Weber-Morris plot described as the macropore diffusion region.

Conversely, in the micropores where the pore size is comparable to the size of adsorbate molecules, diffusion is highly restricted by the presence of pore walls. This diffusion kinetic is described by Fick's law:

$$\frac{\partial C}{\partial t} = \frac{1}{r^2}\frac{\partial}{\partial r}\left(r^2 D_e \frac{\partial C}{\partial r}\right) \tag{4}$$

which can be solved to the following equation in terms of the adsorbate uptake (q) on the assumption that the pores are identical and homogeneously distributed in the spherical adsorbent particles [65,66]:

$$\frac{q}{q_e} = 1 - \frac{6}{\pi^2}\sum_{n=1}^{\infty}\frac{1}{n^2} exp\left(-\frac{n^2\pi^2 D_e t}{R^2}\right) \tag{5}$$

where q_e is the pyridine uptake at equilibrium, D_e is the effective diffusion coefficient of the adsorbate molecules confined within the pore space, r is the coordinate, n is an integer and R is the radius of the

adsorbent particle. Equation 5 can be simplified to give the homogeneous particle diffusion model [34,67] as:

$$q = q_e\sqrt{1 - \exp\left(-\frac{\pi^2 D_e}{R^2}t\right)} \quad (6)$$

The homogeneous particle diffusion model (Equation 6) was subsequently applied to determine the effective diffusion coefficient for pyridine adsorption on MN 200 and MN 500 at various conditions, by making least square fit between this equation and the experimental adsorption kinetic data (q vs t profiles) of the micropore diffusion region indicated by the Weber-Morris plot to meet the minimised average relative deviation in percentage (ARD):

$$ARD\ (\%) = \frac{1}{m}\sum\left|\frac{q_{expt} - q_{calc}}{q_{expt}}\right| \times 100 \quad (7)$$

where m is the number of data point, q_{expt} and q_{calc} are the experimental and calculated pyridine uptakes on the adsorbents. The diameters of the MN 200 and MN 500 studied are in the range of 550-750 µm, so the average adsorbent radii (R) were taken to be 325 µm.

The internal film and homogeneous particle diffusion models, responsible for macropore and micropore diffusion regions respectively, are fitted to the pyridine adsorption kinetics on MN 200 and MN 500, and compared to the experimental adsorption kinetic profiles, shown in Figures 4 and 5. The homogeneous particle diffusion model with the effective diffusion coefficient satisfactorily fits the whole kinetics for MN 200 at temperatures of 35, 45, 55 ^{0}C (this is also where Weber-Morris gave closer-to-zero intercept shown in Figure 1a, which means smaller effect of film diffusion on adsorption kinetics), while the model generally over-predicts the early part of the other kinetics plots, which is associated to the macropores where the internal film diffusion model applies. Conversely, the internal film diffusion model well fits the early part of the plot, whereas it significantly over-predicts for longer adsorption times (shown in Supporting Infornation). This makes it plausible to propose the diffusion mechanisms inside the Macronet adsorbents MN 200 and MN 500 taking into account of:

(i) *internal film diffusion* within the large macropores (where the pore size is much larger than the size of diffusing species) with a film existing between the bulk of the pore and the pore surface;

(ii) *homogeneous particle diffusion* within the much smaller micropores (where the pore size becomes comparable with the size of diffusing species) dominated by collisions with the pore walls.

In order to adsorb onto the macropore surface, the adsorbate will penetrate though a 'film' inside the pores, which is similar to that on the external adsorbent surface but cannot effectively suppressed by external agitation. When the adsorbate diffuses into the micropores, the diffusion pathway is more greatly affected by the pore walls and under this condition the adsorption kinetics is subject to a homogeneous particle diffusion where collisions with the pore walls dominates.

It is shown in Table 2 that there is no significant correlation between the initial pyridine concentration and the adsorption kinetics for MN 200 and MN 500, in terms of internal film diffusion rate constant (k_f) and effective diffusion coefficient (D_e) for the macro- and micropore region, respectively. Conversely, both the two kinetics parameters show an increasing trend with temperature for both MN 200 and MN 500, which is expected as higher temperature increases the rate of molecular motion for the bulk-like liquids as well as for liquid confined in pores. The internal film diffusion rate coefficient and the effective diffusion coefficient for MN 500 are greater, in general, relative to MN 200 at the same condition, implying a faster kinetics for MN 500 in both macro and micropores, which is attributed to the pyridine-surface interaction further enhanced by the functionalisation with sulfonic acid groups on MN 500, despite specific surface area and pore volume of this adsorbent are much smaller than MN 200 [22].

The study clearly shows that a combination of internal film and homogeneous particle diffusion models is appropriate to describe the adsorption kinetics of the Macronet adsorbents exhibiting a bimodal pore size distribution. Using $\delta = D_m/k_f$ with the molecular diffusion coefficient of pyridine in bulk liquid [19] (D_m, the determination will be shown in the following section) gives an estimate of the internal film thickness (δ) in the scale of hundreds of nanometers, which is in line with the macropore size of the Macronet

hypercrosslinked polymers [68]. This confirms that the internal film diffusion resistance would probably be rate-controlling in the large pores also of hundred nanometers in the adsorbent particles.

It is also noted that the identification of internal film diffusion resistance is based on preliminary observation of the negative intercept in Weber-Morris plot, where the transition from internal film diffusion to homogeneous particle diffusion as the rate-controlling mechanism is approximated as the joint between macropore and micropore diffusion regions. However, in the case of a non-negative intercept , although there might also be two or multiple linear regions [59,61], the adsorption kinetics is more likely to be controlled by a homogeneous particle diffusion-like mechanism. This is where the pore size is small enough to sufficiently confine the diffusing adsorbates and the degree of confinement can be revealed from value of the Weber-Morris plot gradient (k) that presents each diffusional region.

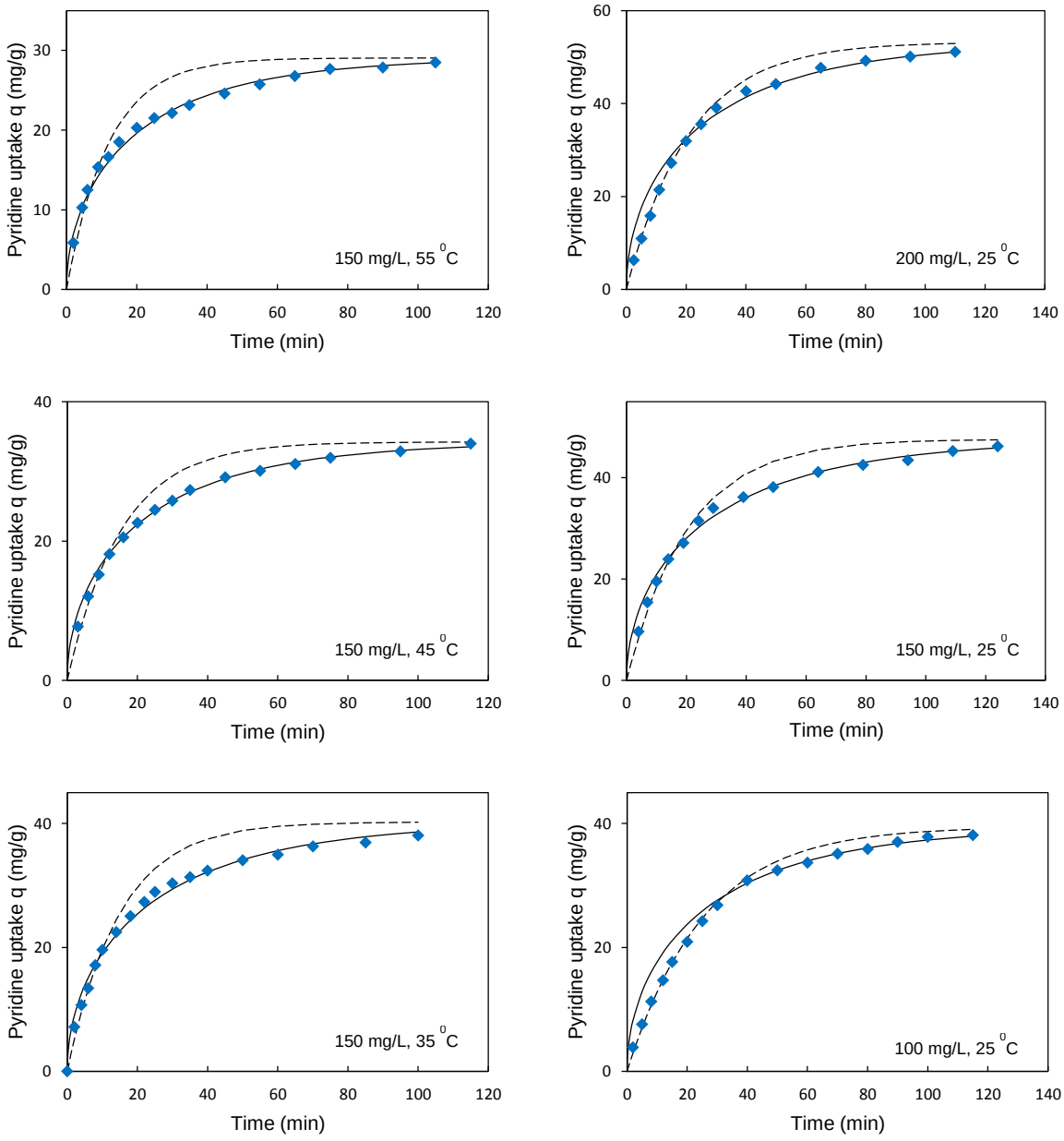

Figure 4. Adsorption kinetics of pyridine on MN 200 from water at various conditions. The blue diamond indicates the experimental data. Dashed line (---) indicates the adsorption kinetics predicted from internal film diffusion model and solid line (-) indicates the adsorption kinetics predicted from homogeneous particle diffusion model. Uncertainty in the experiment is up to $\pm$10%.

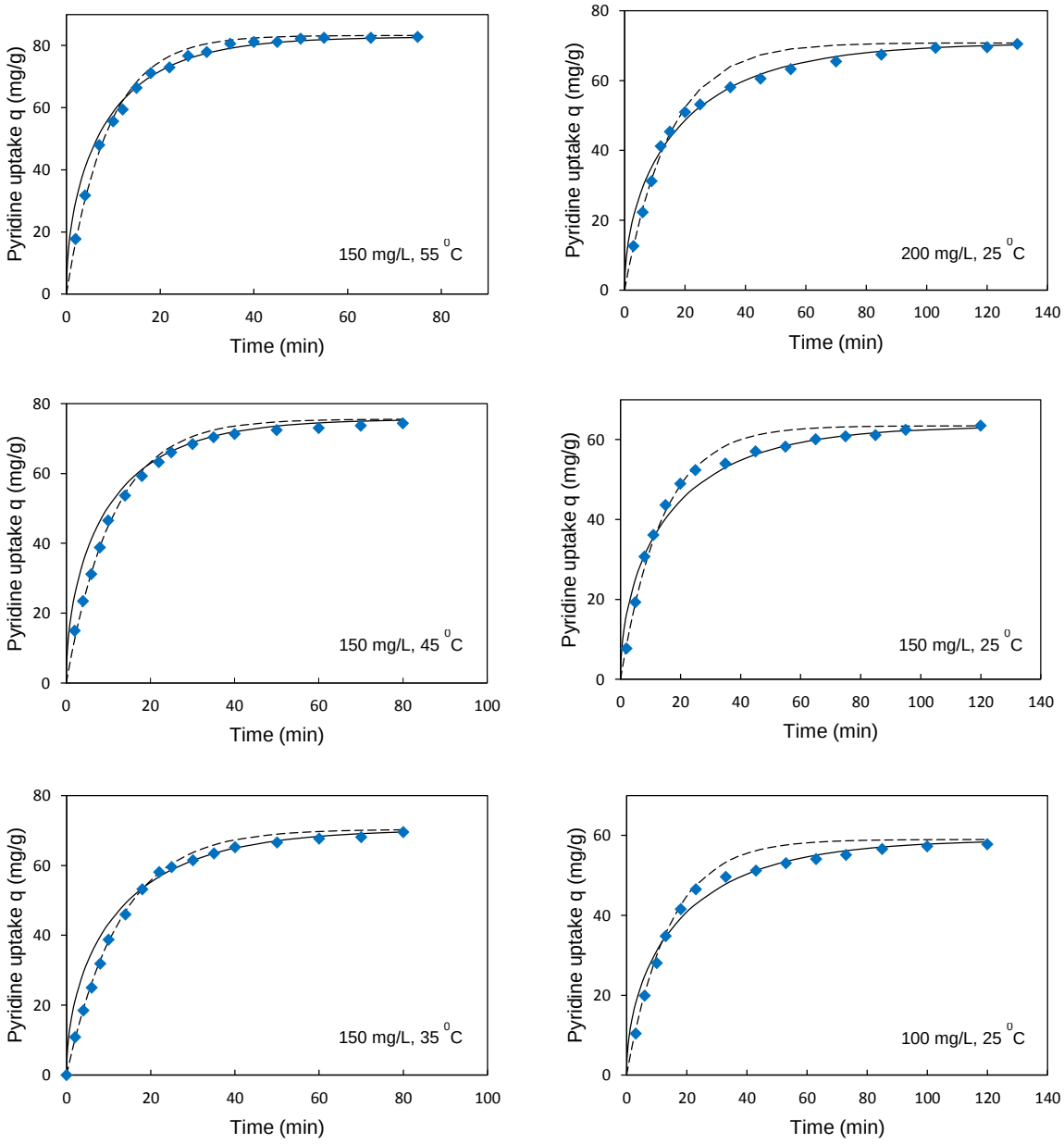

Figure 5. Adsorption kinetics of pyridine on MN 500 from water at various conditions. The blue diamond indicates the experimental data. Dashed line (---) indicates the adsorption kinetics predicted from internal film diffusion model and solid line (-) indicates the adsorption kinetics predicted from homogeneous particle diffusion model. Uncertainty in the experiment is up to $\pm$10%.

Table 2. The film diffusion rate coefficient (k_f) and the effective diffusion coefficient (D_e) for adsorption of pyridine onto MN 200 and MN 500 with different initial pyridine concentrations and temperatures.

Adsorbent	T (^{0}C)	C_0 (mg /L)	k_f (10^{-3}/s)	R^2	D_e (10^{-12} m^2/s)	*ARD (%)*
MN 200	25	100	0.65±0.02	0.998	4.00±0.19	0.63
	25	150	0.81±0.07	0.995	3.81±0.12	1.27
	25	200	0.79±0.02	0.997	4.14±0.14	1.36
	35	150	1.12±0.10	0.990	4.67±0.15	1.82
	45	150	1.08±0.05	0.994	5.01±0.05	0.41
	55	150	1.39±0.08	0.992	5.44±0.08	0.51
MN 500	25	100	1.18±0.07	0.999	5.58±0.23	1.49
	25	150	1.12±0.30	0.993	6.14±0.23	1.75
	25	200	1.21±0.03	0.994	5.72±0.06	0.82
	35	150	1.31±0.02	0.999	8.58±0.24	0.81
	45	150	1.51±0.03	0.997	10.6±0.19	0.62
	55	150	1.90±0.06	0.996	12.5±0.20	0.53

3.3. Pore and surface diffusion

The adsorbent saturated with liquid in pores can effectively be considered as containing two distinct parts with differing molecular dynamics. In the void bulk of the pores, the diffusion behaviour is determined by a pore geometry confinement effect (*i.e.,* the presence of the pore walls reduces the average root mean square displacement of molecules relative to the case of free bulk liquid diffusion), which results in a decrease of diffusion rate compared to that of the free bulk liquid. This effect is denoted as pore diffusion [69]. On the pore surface, the molecular dynamics is altered by liquid-surface interaction (adsorption) as well as limited diffusion path, which can be described as surface diffusion [70].

The pore diffusion coefficient can be measured as the molecular diffusion coefficient of the adsorbate of a solution confined in the tested adsorbent particles using the established PFG-NMR technique. However, the aqueous pyridine solutions studied in this work are at pyridine concentrations of 100-200 mg/L (mole fractions of pyridine of 2.5×10^{-5}-4.5×10^{-5}). These low concentrations make it difficult to measure molecular

diffusivities of pyridine in either the bulk solution or that of the solution inside the polymer porous matrix, because of the overwhelming signal of water together with NMR peak broadening typical of liquid in porous material, which does not allow to detect the pyridine signal. Hence, the pore diffusion coefficients were estimated using the following expression:

$$D_p = D_m \frac{\varepsilon}{\xi} \tag{8}$$

where D_m is the molecular diffusivity of pyridine in the bulk liquid solution, ε is the adsorbent porosity, and ξ is the PFG parameter which is closely related to pore tortuosity [69]. The values of porosity for MN 200 and MN 500 are 59% and 51% taken from the literature [71]. The PFG parameter measures the effect the pore structure has in reducing the diffusivity of guest molecules relative to the free bulk liquid. In order to reflect the structural features of the porous matrix, such values of PFG parameter can be obtained by performing diffusion measurements using weak-interacting molecules, such as hydrocarbons, which have previously been reported for the polymers used in this work using PFG-NMR [22]: averagely 3.4$\pm$0.1 and 2.4$\pm$0.1 for macropores and 14.7$\pm$1.7 and 12.8$\pm$1.3 for micropores of MN 200 and MN 500, respectively.

The molecular diffusivities of pyridine in the aqueous solutions as bulk liquid were extracted from the mutual diffusivity profile of pyridine-water on the basis that the molecular diffusivity of pyridine in the concentration range (100-200 mg/L) can be assumed constant and equal to the molecular diffusivity of pyridine at infinite dilution, which is equivalent in value to the mutual diffusivity at its infinite dilution [72]. Thus the molecular diffusivity of pyridine (D_m) can be determined by extrapolating the mutual diffusivity profile to the case where pyridine is at infinite dilution on the ground that mutual diffusivity profile of the binary liquid system is smooth and continuous [73]. Figure 7 shows the extrapolation of mutual diffusion coefficients to infinite dilution using polynomials for the pyridine-water system at 2, 13, 25, 40 ^{0}C. A linear dependence was found from the extrapolated mutual diffusivity of pyridine at infinite dilution; hence the molecular diffusivities of pyridine at desired temperature of 25, 35, 45 and 55 ^{0}C can be calculated according to the best fitted straight line, shown in Figure 8.

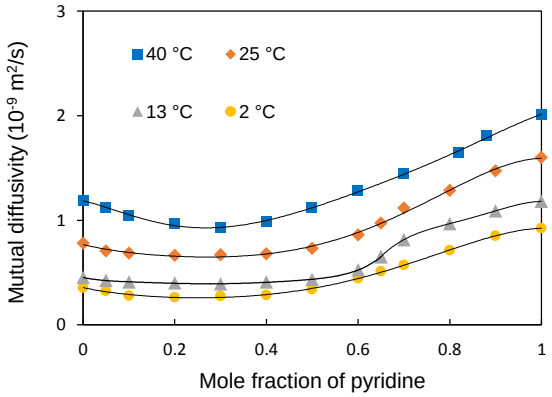

Figure 7. Mutual diffusivity-composition profiles of pyridine-water system at 2, 13, 25 and 40 ^{0}C (data accessed from the Dechema database). The solid lines indicate best-fit polynomials extrapolating the mutual diffusion coefficient to data points at infinite dilution.

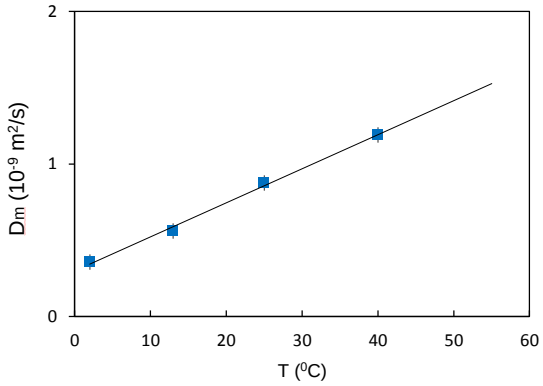

Figure 8. Molecular diffusivity of pyridine at infinite dilution in aqueous solutions (D_m) at various temperatures. The blue squares are from the extrapolated diffusion coefficients for pyridine at infinite dilution from the mutual diffusion profiles shown in Figure 7. The solid line indicates best-fit straight line for interpolation and extrapolation. Vertical bars indicate error in the determined molecular diffusivities.

The molecular diffusivity (D_m) of pyridine in the free bulk aqueous solutions and pore diffusion coefficient (D_p) of pyridine in macropores and micropores of MN 200 and MN 500, respectively' from the aqueous solutions are shown in Table 3. The marked reduction of pore size reasonably explains the significant decrease of diffusion coefficients moving from macropores to micropores. In macropores, the diffusion kinetics is dominated by molecule-molecule collisions and the reduction in diffusivity is due to a reduced average molecular displacement caused by a geometrical confinement. In the micropores, the size of diffusing molecules becomes comparable to that of the pore and molecule-wall collisions become the

dominant effect, which significantly slows down the overall diffusion processes. In such a case, the diffusion mechanism can be ascribed to a surface diffusion process [74,75].

Table 3. Molecular (D_m) and pore (D_p) diffusion coefficients of infinitely diluted pyridine in aqueous solutions within MN 200 and MN 500 adsorbents.

T (^{0}C)	D_m (10^{-10} m^2/s)	D_p (10^{-10} m^2/s)			
		Macropore		Micropore	
		MN200	MN500	MN 200	MN 500
25	8.80±0.46	1.53±0.10	1.87±0.15	0.35±0.04	0.35±0.04
35	10.8±0.6	1.87±0.12	2.30±0.18	0.43±0.05	0.43±0.05
45	13.2±0.7	2.29±0.15	2.82±0.22	0.53±0.07	0.53±0.06
55	15.3±0.7	2.66±0.17	3.25±0.25	0.61±0.08	0.61±0.07

Surface diffusion can be treated as an independent flow in addition to pore diffusion in the bulk void of the adsorbent in contributing to the overall flux of the adsorbate [46,75], which will be more prominent in the micropores, where the motion of the adsorbate is more affected by the pore walls. The total flux (J) in the micropores using Fick' theories can be expressed as follows:

$$J = -\varepsilon D_p \frac{\partial C}{\partial r} - (1-\varepsilon) D_s \frac{\partial C_s}{\partial r} \tag{9}$$

where D_p and D_s are the pore and surface diffusion coefficients respectively, C and C_s are the concentrations of adsorbate in bulk external liquid and on the adsorbent surface per unit volume, respectively. The corresponding mass balance equation within the pore of a spherical adsorbent is:

$$\varepsilon \frac{\partial C}{\partial t} + (1-\varepsilon) \frac{\partial C_s}{\partial t} + \frac{1}{r^2} \frac{\partial}{\partial r} (r^2 J) = 0 \tag{10}$$

Given:

$$\frac{\partial C_s}{\partial r} = \frac{\partial C_s}{\partial C} \frac{\partial C}{\partial r}, \qquad \frac{\partial C_s}{\partial t} = \frac{\partial C_s}{\partial C} \frac{\partial C}{\partial t} \tag{11}$$

Equation 10 is substituted by Equations 9 and 11 to be:

$$\left[\varepsilon + (1-\varepsilon)\frac{\partial C_s}{\partial C}\right]\frac{\partial C}{\partial t} = \frac{1}{r^2}\frac{\partial}{\partial r}\left(r^2\left[\varepsilon D_p + (1-\varepsilon)D_s\frac{\partial C_s}{\partial C}\right]\frac{\partial C}{\partial r}\right) \quad (12)$$

Recalling that the intraparticle diffusion of the adsorption process can be briefly expressed as Fick's second law in terms of the effective diffusion coefficient (D_e) in Equation 4. Substituting Equation 12 into Equation 4, the effective diffusion coefficient can be written as a combination of pore and surface diffusion coefficients as:

$$D_e = \frac{\varepsilon D_p + (1-\varepsilon)\frac{\partial C_s}{\partial C}D_s}{\varepsilon + (1-\varepsilon)\frac{\partial C_s}{\partial C}} \quad (13)$$

In a preferable adsorption process, the amount of adsorbate confined in the bulk pore void is negligible compared to that adsorbed onto the solid phase. Therefore, it is reasonable to assume the total adsorbate uptake (q) as equal to the uptake on the solid phase, thus can be written as:

$$q = \frac{C_s}{\rho_s} \quad (14)$$

where ρ_s is the solid phase density of the adsorbent and will be taken as 1.15 and 1.57 g/cm^3, respectively, for MN 200 and MN 500 from the literature [64,71]. Furthermore, surface diffusion will more greatly affect the micropore diffusion region where is close to the state of adsorption equilibrium; the derivative of q over C can be approximated as:

$$\frac{\partial q}{\partial C} = \frac{\partial q_e}{\partial C_e} \quad (15)$$

where q_e and C_e denotes pyridine uptake and pyridine concentration in bulk liquid at equilibrium. Substituting Equations 14 and 15 into Equation 13, one has:

$$D_e = \frac{\varepsilon D_p + (1-\varepsilon)\rho_s\frac{\partial q_e}{\partial C_e}D_s}{\varepsilon + (1-\varepsilon)\rho_s\frac{\partial q_e}{\partial C_e}} \quad (16)$$

where $\partial q_e/\partial C_e$ can be determined form the adsorption isotherms, for which Langmuir and Freundlich models have been shown to be the best fit models for pyridine adsorption on MN 200 and MN 500, respectively, at 25-55 ^{0}C [22]. Thus for MN 200 and MN 500 we have, respectively:

$$\frac{\partial q_e}{\partial C_e} = \frac{q_m K_L}{(1+K_L C_e)^2} \tag{17}$$

$$\frac{\partial q_e}{\partial C_e} = \frac{1}{\alpha} K_F C_e^{\frac{1}{\alpha}-1} \tag{18}$$

where q_m and K_L are the maximum uptake and the Langmuir constant, respectively, and α and K_F are the exponent and Freundlich constant respectively.

A similar relation of effective diffusion coefficient to pore and surface diffusion coefficients to Equation 16 have been shown by McKay and co-workers [50] and Valderrama and co-workers [58,64], where the Langmuir model was applied for the adsorption isotherms. In this work, with the effective diffusion coefficient (D_e) determined from the homogeneous particle diffusion model and pore diffusion coefficient (D_p) from the PFG parameters for the micropore diffusion region, surface diffusion coefficients for pyridine adsorption on MN 200 and MN 500 from aqueous solutions were calculated using Equation 16 with a best-fit isotherm model (Equation 17 or 18) for various initial pyridine concentrations and temperatures, shown in Table 4. The values of surface diffusion coefficient are close to the results for pyridine adsorption from aqueous solutions on granular activated carbon (*e.g.,* D_s of 6.9×10^{-12} m^2/s with C_0 of 100 mg/L at 35 ^{0}C) reported by Ocampo-Perez et al. [9], and show the same order of magnitude of effective diffusion coefficients (in Table 2) but much lower than the according pore diffusion coefficients (in Table 3), which indicates a significant effect of surface diffusion on the micropore adsorption kinetics. A trend shows the surface diffusion coefficient increases with temperature from 25 to 55 ^{0}C and this is more prominent for MN 500, supporting the hypothesis that surface diffusion is an activated mass transfer process, where the increase of temperature facilitates molecular hopping between distinct, energetically favourable adsorption sites on the surface [47,75,76]. The surface diffusion coefficient was reported to increase with

adsorbent loading, hence is expected to increase with initial adsorbent concentration according to Darken theory [77], although this trend is not well defined in our case, possibly due to the small concentration differences (100 to 200 mg/L).

Table 4. Surface diffusion coefficients for pyridine adsorption on MN 200 and MN 500 from water calculated using Equation 16 with $\partial q_e/\partial C_e$ for MN 200 from Langmuir isotherm model and $\partial q_e/\partial C_e$ for MN 500 from Freundlich isotherm model.

Adsorbent	T (^{0}C)	C_0 (mg/L)	C_e (mg/L)	$\partial q_e/\partial C_e$ (L/g)	D_s (10^{-12} m^2/s)
MN 200	25	100	50.2	0.396	3.90±0.19
	25	150	89.7	0.205	3.62±0.13
	25	200	134	0.118	3.81±0.15
	35	150	103	0.213	4.44±0.15
	45	150	109	0.190	4.70±0.06
	55	150	114	0.188	5.06±0.09
MN 500	25	100	29.1	0.420	5.53±0.23
	25	150	70.3	0.214	6.05±0.23
	25	200	111	0.151	5.60±0.07
	35	150	66.1	0.236	8.49±0.24
	45	150	57.7	0.285	10.5±0.2
	55	150	45.3	0.327	12.4±0.2

Equation 16 can be generalised as:

$$D_e = (1 - x_s)D_p + x_s D_s \tag{19}$$

giving:

$$x_s = \frac{(1-\varepsilon)\rho_s \frac{\partial q_e}{\partial C_e}}{\varepsilon + (1-\varepsilon)\rho_s \frac{\partial q_e}{\partial C_e}} \tag{20}$$

where x_s denotes the relative weight of surface diffusion coefficients, and ratio $x_s D_s/D_e$ can be used as an indication of relative contribution of surface diffusion to the adsorption kinetics in the micropores. Values of $x_s D_s/D_e$ in percentage are shown in Figure 9 for pyridine adsorption on MN 200 and MN 500 from aqueous solutions at various temperature and initial pyridine concentration. The ratio $x_s D_s/D_e$ decreases

with initial pyridine concentration for both adsorbents, which is expected as increasing the concentration, more pyridine molecules are likely to occupy the pore voids, hence contributing to pore diffusion rather than surface diffusion. However, the ratio shows a decreasing and an increasing trend as a function of temperature, respectively, for MN 200 and MN 500, which is similar to the temperature dependence of adsorption isotherms reported in Part 1 [22]. In particular, adsorption on MN 200 is an exothermic process and therefore an increase in temperature decreases the pyridine uptake over the surface, hence reducing the surface diffusion contribution. Conversely, on MN 500, which is an endothermic process, an increase in temperature increases the adsorption capacity of the surface, hence increasing the surface diffusion contribution. This suggests a relationship between the adsorption uptake and the contribution of surface diffusion.

Surface diffusion coefficient in general contributes over 90 % to the effective diffusion coefficient in the micropore space, revealing the significance of surface diffusion in the intraparticle diffusion mechanism. As to compare between MN 200 and MN 500, greater surface diffusion values are observed for MN 500 relative to MN 200. This might be because the presence of functionalised sulfonic acid groups on the MN 500 surface lowers the energy barrier of molecular hopping due to an increased surface coverage, hence enhancing the diffusion rate onto the surface [78], as well as increasing surface diffusion contribution to the adsorption kinetics in the micropores, which agrees with its higher pyridine uptake from aqueous solutions. These results give new insights and a better understanding into the adsorption kinetics of the Macronet adsorbents where the pore structures affect the diffusion mechanisms.

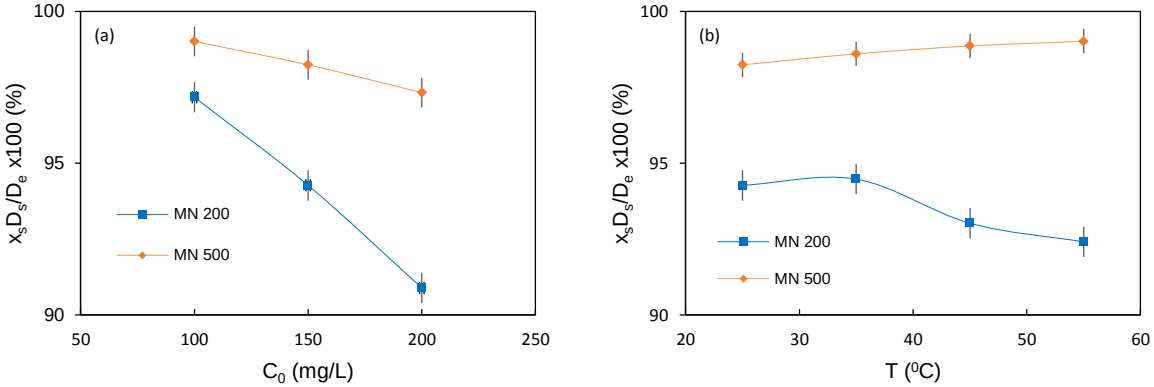

Figure 9. Relative contribution of surface diffusion to the effective diffusion coefficient in terms of the ratio x_sD_s/D_e in percentage for pyridine adsorption on MN 200 and MN 500 by (a) varying initial pyridine concentration at 25 ^{0}C and (b) varying temperature at initial pyridine concentration of 150 mg/L. The vertical bars indicate error estimates on the calculated ratios.

4. Conclusions

The adsorption kinetics of pyridine on Macronet adsorbents MN 200 and MN 500 were studied at different initial pyridine concentrations and temperatures. The kinetics was investigated using Weber-Morris plots, revealing influence of film diffusion and intraparticle diffusion resistances, and showed two distinctive diffusion regimes, attributed as macropore and micropore diffusion regions which are linked to the bimodal pore size property of the adsorbents. The adsorption mechanisms in the pores were characterised as film diffusion on the internal macropore surface (bulk-like behaviour where diffusion is dominated by molecule-molecule collisions) and intraparticle diffusion in micropores described by homogeneous particle diffusion model with effective diffusion coefficient (diffusion dominated by molecule-wall collisions).

With the proposed diffusion mechanisms, the relative importance of pore and surface diffusions are noted in contributing to the intraparticle diffusion process in the micropores of the adsorbent particles. The pore diffusion, only considering the geometrical confinement of the adsorbent geometry, was estimated using PFG-NMR results and the molecular diffusivity of the adsorbate in bulk liquid. The surface diffusion coefficient was calculated from its relation to pore and effective diffusion coefficients together with the

adsorption isotherms data. Greater surface diffusion contribution is found for MN 500, which agrees with its better adsorption performance of pyridine adsorption from aqueous solutions.

Acknowledgements

Carmine D'Agostino would like to acknowledge Wolfson College, Cambridge, for supporting his research activities.

5. References

[1] H. Bouyarmane, S. El Asri, A. Rami, C. Roux, M.A. Mahly, A. Saoiabi, T. Coradin, A. Laghzizil, Pyridine and phenol removal using natural and synthetic apatites as low cost sorbents: influence of porosity and surface interactions, J. Hazard. Mater. 181 (2010) 736–41.

[2] G.K. Sims, E.J. O'Loughlin, R.L. Crawford, Degradation of pyridines in the environment, Crit. Rev. Environ. Control. 19 (1989) 309–340.

[3] K.V. Padoley, S.N. Mudliar, R.A. Pandey, Heterocyclic nitrogenous pollutants in the environment and their treatment options—an overview, Bioresour. Technol. 99 (2008) 4029–4043.

[4] J. Li, W. Cai, J. Cai, The characteristics and mechanisms of pyridine biodegradation by Streptomyces sp., J. Hazard. Mater. 165 (2009) 950–4.

[5] J. Kaiser, Y. Feng, J.-M. Bollag, Microbial metabolism of pyridine, quinoline, acridine, and their derivatives under aerobic and anaerobic conditions, Microbiol. Mol. Biol. Rev. 60 (1996) 483–498.

[6] N.R. Singha, S.K. Ray, Removal of Pyridine from Water by Pervaporation Using Crosslinked and Filled Natural Rubber Membranes, J. Appl. Polym. Sci. 124 (2012) E99–E107.

[7] R. Andreozzi, A. Insola, V. Caprio, M.G. D'Amore, Ozonation of pyridine in aqueous solution: mechanistic and kinetic aspects, Water Res. 25 (1991) 655–659.

[8] C. Bag, S. Krishnamurthy, C. Bhattacharjee, Treatment of wastewater containing pyridine released from N,N'-dichlorobis(2,4,6-trichlorophenyl) urea (CC2) plant by advanced oxidation, J. Environ. Prot. Sci. 3 (2009) 34–40.

[9] R. Ocampo-Perez, R. Leyva-Ramos, P. Alonso-Davila, J. Rivera-Utrilla, M. Sanchez-Polo, Modeling adsorption rate of pyridine onto granular activated carbon, Chem. Eng. J. 165 (2010) 133–141.

[10] D. Mohan, K.P. Singh, S. Sinha, D. Gosh, Removal of pyridine from aqueous solution using low cost activated carbons derived from agricultural waste materials, Carbon N. Y. 42 (2004) 2409–2421.

[11] P. Alonso-Davila, O.L. Torres-Rivera, R. Leyva-Ramos, R. Ocampo-Perez, Removal of pyridine from aqueous solution by adsorption on an activated carbon cloth, Clean Soil, Air, Water. 40 (2012) 45–53.

[12] D.H. Lataye, I.M. Mishra, I.D. Mall, Pyridine sorption from aqueous solution by rice husk ash (RHA) and granular activated carbon (GAC): parametric, kinetic, equilibrium and thermodynamic aspects, J. Hazard. Mater. 154 (2008) 858–870.

[13] Y. Bai, Q. Sun, R. Xing, D. Wen, X. Tang, Removal of pyridine and quinoline by bio-zeolite composed of mixed degrading bacteria and modified zeolite, J. Hazard. Mater. 181 (2010) 916–22.

[14] M.M. Broholm, K. Broholm, E. Arvin, Sorption of heterocyclic compounds on natural clayey till, J. Contam. Hydrol. 39 (1999) 183–200.

[15] J. Bokhove, B. Schuur, A.B. de Haan, Resin screening for the removal of pyridine-derivatives from waste-water by solvent impregnated resin technology, React. Funct. Polym. 73 (2013) 595–605.

[16] Y. Zhang, D. Li, Adsorption of pyridine on post-crosslinked fiber, J. Sci. Indistrial Res. 69 (2010) 73–76.

[17] M.J. Kim, S.M. Park, S.-J. Song, J. Won, J.Y. Lee, M. Yoon, K. Kim, G. Seo, Adsorption of pyridine onto the metal organic framework MIL-101., J. Colloid Interface Sci. 361 (2011) 612–617.

[18] Z. Hasan, M. Tong, B.K. Jung, I. Ahmed, C. Zhong, S.H. Jhung, Adsorption of pyridine over amino-functionalized metal− organic frameworks: attraction via hydrogen bonding versus base−base repulsion, J. Phys. Chem. C. 118 (2014) 21049–21056.

[19] C.-F. Chang, C.-Y. Chang, K.-E. Hsu, S.-C. Lee, W. Höll, Adsorptive removal of the pesticide methomyl using hypercrosslinked polymers, J. Hazard. Mater. 155 (2008) 295–304.

[20] L.J. Abbott, C.M. Colina, Formation of Microporosity in Hyper-Cross-Linked Polymers, Macromolecules. 47 (2014) 5409–5415.

[21] E. Andrijanto, E. A. Dawson, D.R. Brown, Hypercrosslinked polystyrene sulphonic acid catalysts for the esterification of free fatty acids in biodiesel synthesis, Appl. Catal. B Environ. 115-116 (2012) 261–268.

[22] Q. Zhu, G.D. Moggridge, M. Ainte, M.D. Mantle, L.F. Gladden, C. D'Agostino, Adsorption of pyridine from aqueous solutions by polymeric adsorbents MN 200 and MN 500. Part 1: Adsorption performance and PFG-NMR studies, Chem. Eng. J. In press.

[23] G. McKay, S.J. Allen, F. McCovey, J.H.R. Walters, External mass transfer and homogeneous solid-phase diffusion effects during the adsorption of dyestuffs, Ind. Eng. Chem. Process Des. Dev. 23 (1984) 221–226.

[24] C. Valderrama, X. Gamisans, X. de las Heras, A. Farrán, J.L. Cortina, Sorption kinetics of polycyclic aromatic hydrocarbons removal using granular activated carbon: intraparticle diffusion coefficients, J. Hazard. Mater. 157 (2008) 386–96.

[25] Y.S. Ho, G. McKay, A comparison of chemisorption kinetic models applied to pollutant removal on various sorbents, Process Saf. Environ. Prot. 76 (1998) 332–340.

[26] M.T. Yagub, T.K. Sen, S. Afroze, H.M. Ang, Dye and its removal from aqueous solution by adsorption: a review., Adv. Colloid Interface Sci. 209 (2014) 172–84.

[27] J. Ma, F. Yu, L. Zhou, L. Jin, M. Yang, J. Luan, Y. Tang, H. Fan, Z. Yuan, J. Chen, enhanced adsorptive removal of methyl orange and methylene blue from aqueous solution by alkali-activated multiwalled carbon nanotubes, Appl. Mater. Interfaces. 4 (2012) 5749–5760.

[28] A.E. Ofomaja, Intraparticle diffusion process for lead (II) biosorption onto mansonia wood sawdust, Bioresour. Technol. 101 (2010) 5868–5876.

[29] W.H. Cheung, Y.S. Szeto, G. McKay, Intraparticle diffusion processes during acid dye adsorption onto chitosan, Bioresour. Technol. 98 (2007) 2897–2904.

[30] D. Reichenberg, Properties of ion-exchange resins in relation to their Structure. III. Kinetics of exchange, J. Am. Chem. Soc. 75 (1953) 589–597.

[31] Z. Tao, J. Niu, Shell-progressive model with changing bulk concentration and exchanger volume in ion exchange, Solvent Extr. Ion Exch. 8 (1990) 99–115.

[32] A. Wilczak, T.M. Keinath, Kinetics of sorption and desorption of copper (II) and lead (II) on activated carbon, Water Environ. Res. 65 (1993) 238–244.

[33] J. Serarols, J. Poch, I. Villaescusa, Determination of the effective diffusion coefficient of Zn (II) on a macroporous resin XAD-2 impregnated with di-2-ethylhexyl phosphoric acid (DEHPA): Influence of metal concentration and particle size, React. Funct. Polym. 48 (2001) 53–63.

[34] M. Balsamo, F. Montagnaro, Fractal-like Vermeulen kinetic equation for the description of diffusion-controlled adsorption dynamics, J. Phys. Chem. C. 119 (2015) 8781–8785.

[35] G. McKay, Solution to the homogeneous surface diffusion model for batch adsorption systems using orthogonal collocation, Chem. Eng. J. 81 (2001) 213–221.

[36] G. Pan, Adsorption kinetics in natural waters: a generalised ion-exchange model, in: A. Dabrowski (Eds.), Studies in Surface Science and Catalysis, Elsevier, Amsterdam, 1998, pp. 745–761.

[37] V. Russo, R. Tesser, M. Trifuoggi, M. Giugni, M. Di Serio, A dynamic intraparticle model for fluid–solid adsorption kinetics, Comput. Chem. Eng. 74 (2015) 66–74.

[38] V. Russo, R. Tesser, D. Masiello, M. Trifuoggi, M. Di Serio, Further verification of adsorption dynamic intraparticle model (ADIM) for fluid–solid adsorption kinetics in batch reactors, Chem. Eng. J. 283 (2016) 1197–1202.

[39] R.G. Peel, A. Benedek, C.M. Crowe, A branched pore kinetic model for activated carbon adsorption, AIChE J. 27 (1981) 26–32.

[40] S. Karthikeyan, B. Sivakumar, Film and pore diffusion modeling for adsorption of reactive red 2 from aqueous solution on to activated carbon prepared from bio-diesel industrial waste, E-Journal Chem. 7 (2010) 175–185.

[41] Y. Wang, H. Zhou, F. Yu, B. Shi, H. Tang, Fractal adsorption characteristics of complex molecules on particles-A case study of dyes onto granular activated carbon (GAC), Colloids Surfaces A Physicochem. Eng. Asp. 299 (2007) 224–231.

[42] S. Wang, Z. Ma, H. Yao, Fractal diffusion model used for diffusion in porous material within limited volume of stiff container, Chem. Eng. Sci. 64 (2009) 1318–1325.

[43] Y. Matsui, N. Ando, H. Sasaki, T. Matsushita, K. Ohno, Branched pore kinetic model analysis of geosmin adsorption on super-powdered activated carbon, Water Res. 43 (2009) 3095–3103.

[44] H. Komiyama, J.M. Smith, Surface diffusion in liquid-filled pores, AIChE J. 20 (1974) 1110–1117.

[45] K. Miyabe, G. Guiochon, Measurement of the parameters of the mass transfer kinetics in high performance liquid chromatography, J. Sep. Sci. 26 (2003) 155–173.

[46] I. Medved, R. Cerný, Surface diffusion in porous media: A critical review, Microporous Mesoporous Mater. 142 (2011) 405–422.

[47] A. Kapoor, R.T. Yang, Contribution of concentration-dependent surface diffusion to rate of adsorption, Chem. Eng. Sci. 46 (1991) 1995–2002.

[48] X. Hu, D.D. Do, G.N. Rao, Experimental concentration dependence of surface diffusivity of hydrocarbons in activated carbon, 49 (1994) 2145–2152.

[49] X. Hu, D.D. Do, Multicomponent adsorption kinetics of hydrocarbons onto activated carbon: effect of adsorption equilibrium equations, Chem. Eng. Sci. 47 (1992) 1715–1725.

[50] C. Hui, B. Chen, G. McKay, Pore-surface diffusion model for batch adsorption processes, Langmuir. 19 (2003) 4188–4196.

[51] J.L. Cortina, A. Warshawsky, N. Kahana, V. Kampel, C.H. Sampaio, R.M. Kautzmann, Kinetics of goldcyanide extraction using ion-exchange resins containing piperazine functionality, React. Funct. Polym. 54 (2003) 25–35.

[52] W.J. Weber, J.C. Morris, Kinetics of adsorption on carbon from solution, J. Sanit. Eng. Div. 89 (1963) 31–60.

[53] G. McKay, V.J.P. Poots, Kinetics and diffusion processes in colour removal from effluent using wood as an adsorbent, J. Chem. Tech. Biotechnol. 30 (1980) 279–292.

[54] A. Zikanova, M. Billow, H. Schlodder, Intracrystalline diffusion of benzene in ZSM-5 and silicalite, Zeolites. 7 (1987) 115–118.

[55] G. McKay, B. Al-Duri, Study of the mechanism of pore diffusion in batch adsorption systems, J.Chem.Tech. BIotechnol. 48 (1990) 269–285.

[56] G. McKay, The adsorption of dyestuffs from aqueous solutions using activated carbon. iii. Intraparticle diffusion processes, J. Chem. Technol. Biotechnol. 33A (1983) 196–204.

[57] F.-C. Wu, R.-L. Tseng, R.-S. Juang, Initial behavior of intraparticle diffusion model used in the description of adsorption kinetics, Chem. Eng. J. 153 (2009) 1–8.

[58] C. Valderrama, J.L. Cortina, A. Farran, X. Gamisans, F.X. de las Heras, Kinetic study of acid red “dye” removal by activated carbon and hyper-cross-linked polymeric sorbents Macronet Hypersol MN200 and MN300, React. Funct. Polym. 68 (2008) 718–731.

[59] P. Liao, S. Yuan, W. Xie, W. Zhang, M. Tong, K. Wang, Adsorption of nitrogen-heterocyclic compounds on bamboo charcoal: kinetics, thermodynamics, and microwave regeneration, J. Colloid Interface Sci. 390 (2013) 189–95.

[60] D. Rameshraja, V.C. Srivastava, J.P. Kushwaha, I.D. Mall, Quinoline adsorption onto granular activated carbon and bagasse fly ash, Chem. Eng. J. 181-182 (2012) 343–351.

[61] H. Zhang, A. Li, J. Sun, P. Li, Adsorption of amphoteric aromatic compounds by hyper-cross-linked resins with amino groups and sulfonic groups, Chem. Eng. J. 217 (2013) 354–362.

[62] V.V. Azanova, J. Hradil, Sorption properties of macroporous and hypercrosslinked copolymers, React. Funct. Polym. 41 (1999) 163–175.

[63] E. Karounou, Removal of endocrine disruptors by activated carbons and hypercrosslinked polymeric adsorbents, 2004.

[64] C. Valderrama, J.I. Barios, M. Caetano, A. Farran, J.L. Cortina, Kinetic evaluation of phenol/aniline mixtures adsorption from aqueous solutions onto activated carbon and hypercrosslinked polymeric resin (MN200), React. Funct. Polym. 70 (2010) 142–150.

[65] G.E. Boyd, A.W. Adamson, L.S. Myers, The exchange adsorption of ions from aqueous solutions by organic zeolites. II. Kinetics, J. Am. Chem. Soc. 69 (1947) 2836-2847.

[66] S.A.M. Eagle, J.W. Scott, Liquid Phase Adsorption Equilibria and Kinetics, Ind. Eng. Chem. 42 (1950) 1287-1294.

[67] T. Vermeulen, Theory for irreversible and constant-pattern solid diffusion, Ind. Eng. Chem. 45 (1953) 1664–1670.

[68] N.A. Penner, P.N. Nesterenko, M.M. Hyin, M.P. Tsyurupa, V.A. Davankov, Investigation of the properties of hypercrosslinked polystyrene as a stationary phase for high-performance liquid chromatography, Chromatographia. 50 (1999) 611–620.

[69] C. D'Agostino, J. Mitchell, L.F. Gladden, M.D. Mantle, Hydrogen bonding network disruption in mesoporous catalyst supports probed by PFG-NMR diffusometry and NMR relaxometry, J. Phys. Chem. C. 116 (2012) 8975–8982.

[70] D. Weber, A.J. Sederman, M.D. Mantle, J. Mitchell, L.F. Gladden, Surface diffusion in porous catalysts., Phys. Chem. Chem. Phys. 12 (2010) 2619–24.

[71] D.S. Stefan, I. Pincovschi, Adsorption of phenol and its chlorinated derivatives from waste waters using hypercrosslinked polymers, Rev. Chim. 64 (2013) 1381–1384.

[72] Q. Zhu, C. D'Agostino, M. Ainte, M.D. Mantle, L.F. Gladden, O. Ortona, L. Paduano, D. Ciccarelli, G.D. Moggridge, Prediction of mutual diffusion coefficients in binary liquid systems with one self-associating component from viscosity data and intra-diffusion coefficients at infinite dilution, Chem. Eng. Sci. 147 (2016) 118–127.

[73] Q. Zhu, G.D. Moggridge, C. D'Agostino, A local composition model for the prediction of mutual diffusion coefficients in binary liquid mixtures from tracer diffusion coefficients, Chem. Eng. Sci. 132 (2015) 250–258.

[74] W. Fritz, W. Merk, E.U. Schlunder, Competitive adsorption of two dissolved organics onto activated carbon-II, Chem. Eng. Sci. 36 (1981) 731–741.

[75] A. Kapoor, R.T. Yang, C. Wong, Surface diffusion, Catal. Rev. 31 (1989) 129–214.

[76] Y.D. Chen, R.T. Yang, Concentration dependence of surface diffusion and zeolitic diffusion, AIChE J. 37 (1991) 1579–1582.

[77] H.D. Do, D.D. Do, I. Prasetyo, On the surface diffusion of hydrocarbons in microporous activated carbon, Chem. Eng. Sci. 56 (2001) 4351–4368.

[78] R. Valiullin, P. Kortunov, J. Kärger, V. Timoshenko, Surface self-diffusion of organic molecules adsorbed in porous silicon, J. Phys. Chem. B. 20 (2005) 5746–5752.